

**Experiment title: Microstructures induced by martensitic transformations in Fe and Ti under extreme conditions**

**Experiment number:**  
HC-4360

<b>Beamline:</b> ID15B	<b>Date of experiment:</b> from: 08 June 2021 to: 12 June 2021	<b>Date of report:</b> 28/02/2022
<b>Shifts:</b> 12	<b>Local contact(s):</b> Gaston Garbarino, Tomasz Poreba	<i>Received at ESRF:</i>
<b>Names and affiliations of applicants (* indicates experimentalists):</b> Agnès Dewaele*, CEA DAM Ile de France DPTA/SPMC Bruyères-le-Châtel FR - 91297 ARPAJON Robin Freville*, CEA DAM Ile de France DPTA/SPMC Bruyères-le-Châtel FR - 91297 ARPAJON		

## Report:

### -Objective & expected results-

We planned to characterize the microstructures induced by archetypical martensitic transformations under extremes conditions in Fe ( $\alpha$ - $\gamma$ - $\varepsilon$ ), Ti ( $\alpha$ - $\omega$ ) and Sn ( $\beta$ - $\gamma$ ), in samples which were initially single crystalline. This aims at an understanding of the mesoscale mechanisms of these transformations.

### -Results and conclusions of the study-

Three diamond anvils cells (DAC), shortly described in **Table 1**, have been bought to ESRF. Starting sample were thin foils ( $e = 12 \mu\text{m}$ ) for Iron, heat treated to grow high quality single crystals which were characterized by MEB-EBSD prior to DAC loading, and powder grains with diameter varying from 4 to 8  $\mu\text{m}$  for Titanium and Tin (they were found to be single crystals in a test experiment).

We used Neon as pressure transmitting medium and  $\text{SrB}_4\text{O}_7:\text{Sm}^{2+}$  was placed in the experimental chamber as a pressure gauge [1].

Experiments were carried out at the ID15B beamline, with an X-ray beam focused to a  $3 \times 3 \mu\text{m}$  FWHM spot on the sample with KB mirrors, and cleaned with a pinhole. A vacuum resistive heater was provided by ESRF to perform the first run. Pressure was measured on-line using the luminescence of the gauge. XRD data were collected using a MAR555 detector with a sample to detector distance calibrated with a reference silicon sample; multi-exposures with  $\pm 25^\circ$  rotation of the DAC and  $0.5^\circ$  step were performed, so that we can perform single/multi-crystals analysis of XRD data. Results for the three runs are summarized below.

Run name	Diamond culet diameter ( $\mu\text{m}$ )	Sample	Pressure range (GPa)	Temperature (K)
<i>FeFoil1</i>	500	Fe in Ne	6->15	300->815
<i>FeFoil2</i>	400	Fe in Ne	6->17	Room T
<i>SnTi</i>	400	Sn {3} and Ti {3} in Ne	0->20	Room T

**Table 1:** Conditions of the 3 runs. Numbers between brackets indicate the number of samples in the DAC.

### 1. Run *FeFoil1*: Growth of large $\varepsilon$ -Fe single crystals

In previous runs, we proved the possibility of synthesizing  $\varepsilon$ -Fe single crystals of good quality using  $\alpha$ - $\rightarrow$ - $\gamma$ - $\rightarrow$ - $\varepsilon$  transitions instead of  $\alpha$ - $\rightarrow$ - $\varepsilon$  transition [HC-2783,HC-2180,HC-3402]. One difficulty to use these single crystals for fine measurements (such as IXS) is their small size ( $<20 \mu\text{m}$ ). We tried to increase it by multiple crossing of

the  $\alpha$ - $\gamma$  transition line, as this procedure is described in the literature. We performed two  $\alpha - \gamma$  cycles and then increased the pressure in the stability domain of  $\varepsilon$ -Fe (see **Figure 1**). Unfortunately, this did not produce the large crystals we were expecting. The single crystal XRD data collected during this run will complete the database from runs HC-2783, HC-2180, HC-3402 to measure conditions, orientation relations and twinning deformation for  $\alpha$ - $\gamma$  and  $\gamma$ - $\varepsilon$  transitions [2].

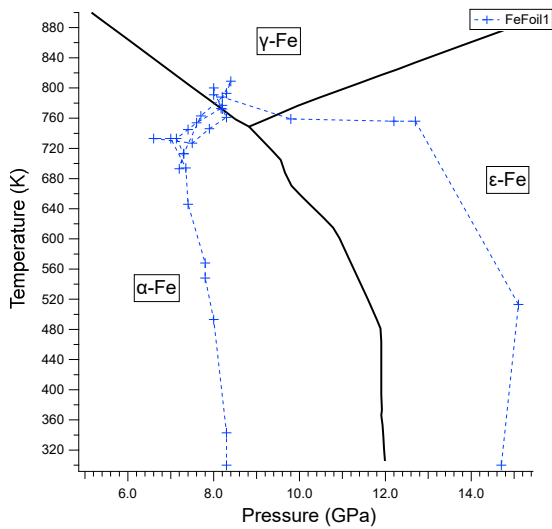


**Figure 1:** P-T path followed during run FeFoil1 (blue dashed lines), plotted in Fe phase diagram from [2].

## 2. Run FeFoil2: deformation and twinning during the $\alpha$ - $\varepsilon$ transition in Iron.

A martensitic transformation produces large elastic stresses that is released with twinning and/or dislocation generation; the plasticity mechanism, which is favoured by the system, has a large impact on the microstructure formed by the transformation. In previous works, we have evidenced that dislocation generation is a major phenomenon in  $\alpha$ -Fe $\leftrightarrow$  $\varepsilon$ -Fe transitions [3,4]. Recent MEB-EBSD *ex-situ* experiments performed in our laboratory suggest that twinning also occurs, mostly in  $\varepsilon$ -Fe but also in  $\alpha$ -Fe. The aim of FeFoil2 run was to detect when twinning is occurring using *in-situ* XRD data. EBSD maps of the sample before and after  $\alpha \rightarrow \varepsilon \rightarrow \alpha$  cycle are presented in **Figure 2**.

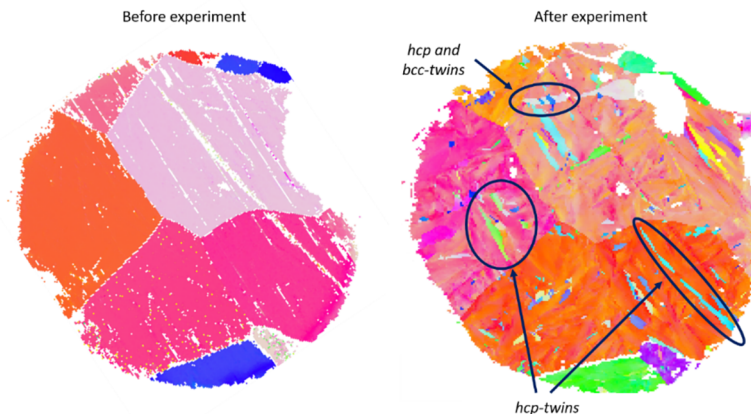


**Figure 2:** EBSD map of FeFoil2 sample (120  $\mu\text{m}$  diameter) collected before and after  $\alpha - \varepsilon - \alpha$  cycle. Overall, the orientation of single crystals is the same (the tone difference is due to a different color scale); color variation within a grain indicates high dislocation densities. Twins produced in hcp ( $\varepsilon$ ) and bcc ( $\alpha$ ) phases are indicated.

XRD mapping of the sample (100 points) was performed at different pressure steps during direct/reverse transitions. Due to the small size of twin variant, we did not find yet its XRD signal; analysis is in progress.

## 3. Run SnTi: transition mechanisms in Titanium and Tin

In Titanium,  $\alpha$  (hcp) to  $\omega$  (hexagonal) phase transition induces an unusual grain enlargement, not understood yet [5]. The  $\beta$ -Sn to *bct*-Sn transition is reported under different conditions under static/dynamic compression/release [6], raising questions on its mechanism. As both transition occur in a similar and limited pressure range, we decided to study both metals in the same DAC, with 3 samples of each metal loaded in the pressure chamber.

One unexpected output of the experiment is the large effect of sample microstructure on the transition conditions. Titanium  $\alpha \rightarrow \omega$  transition onset depends on the starting crystal quality: from 8 GPa for an undeformed crystal to 16 GPa for a deformed crystal (see **Figure 4**). For tin, similar observation with a direct transition between 11 GPa and 12 GPa depending on the crystallinity of the starting crystal. Then, transitions are sharp in pressure for each sample.

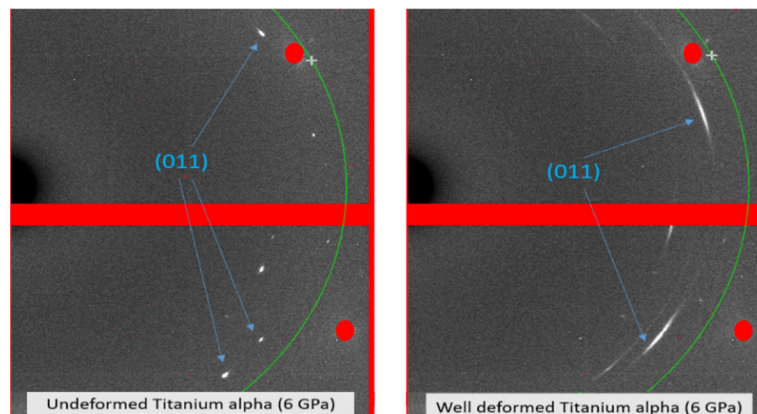


**Figure 4:** Image plate presenting two types of  $\alpha$ -Ti samples at the beginning of the run.

Orientations relations between parent and child phases predicted from crystallography considerations could be observed for some crystals, but not all: Silcock [7] orientation relations for  $\alpha \rightarrow \omega$  Ti transition, and Katzke et al. [8] for  $\beta \rightarrow \gamma$  Sn transition. Twinning occurred during these transformations. The single crystal analysis is still in progress. Our experience with Fe suggests that higher statistics is needed to have a better understanding of the transition mechanism; we thus need more data to corroborate these first results.

#### **-Justification and comments about the use of beam time-**

After alignment of the beamline and calibration by the local contact on the first day, the beam time was used to stabilize P-T conditions in the DAC and collect data for the three cells. The experiment went smoothly; we appreciated the very small spot size of the beamline and the fast and sensitive detector and the accurate sample holder motors.

Data analysis takes time because new methods/programs need to be established/written to treat the new h5 data format.

#### **-References-**

- [1] F. Datchi, F. et al. Improved calibration of the  $\text{SrB}_4\text{O}_7:\text{Sm}^{2+}$  optical pressure gauge: Advantages at very high pressures and high temperatures *J. Appl. Phys.*, 1997, 81, 3333
- [2] A. Dewaele et al., Iron under conditions close to the  $\alpha$ - $\gamma$ - $\epsilon$  triple point, *Appl. Phys. Lett.* 112, 201906, 2018
- [3] A. Dewaele et al. Mechanism of the  $\alpha - \epsilon$  phase transformation in Iron. *Phys. Rev. B* 91 (2015)
- [4] E. Boulard et al. Following the phase transitions of iron in 3D with X-ray tomography and diffraction under extreme conditions. *Acta Mat.*, 2020, 192, pp. 30-39.
- [5] D. Popov et al., Real time study of grain enlargement in Zr under room-T compression across the  $\alpha$  to  $\omega$  phase transition, *Sci. Rep.* 9, 15712, 2019
- [6] R. Briggs et al., Observation of the shock-induced  $\beta$ -sn to b.c.t-Sn transition using time-resolved X-ray diffraction, *J. Synchrotron Rad.* 26, 96, 2019
- [7] J. M. Silcock, *Acta Metall.* 6, 481 (1958); sometimes attributed to A. Rabinkin, M. Talianker, and O. Botstein, *Acta Metall.* 29, 691 (1981).
- [8] H. Katzke et al., Theory of the high-pressure structural phase transitions in Si, Ge, Sn, and Pb, *Physical Review B* 73, 134105, 2006